LAWRENCE
LIVERMORE
NATIONAL
LABORATORY

LLNL-JRNL-630232

Fast Ignition Integrated Experiments and High Gain Point Design

H. Shiraga, H. Nagatomo, W. Theobald, A. A. Solodov, M. Tabak

March 26, 2013

Nuclear Fusion

Disclaimer

Fast Ignition Integrated Experiments and High-Gain Point Design

H. Shiraga[1], H. Nagatomo[1], W. Theobald[2], A. A. Solodov[2], and M. Tabak[3]

[1]*Institute of Laser Engineering, Osaka University, Suita, Osaka 565-0871 Japan*
[2]*Institute for Laser Energetics, University of Rochester, Rochester, NY 14623 USA*
[3]*Lawrence Livermore National Laboratory, Livermore, CA, 94551 USA*

Abstract

Integrated fast ignition experiments were performed at ILE, Osaka, and LLE, Rochester, in which a nanosecond driver laser implodes a deuterated plastic shell in front of the tip of a hollow metal cone and an intense ultrashort-pulse laser is injected through the cone to heat the compressed plasma. Based on the initial successful results of fast electron heating of cone-in-shell targets, large energy short-pulse laser beam lines were constructed and became operational: OMEGA-EP at Rochester and LFEX at Osaka. Neutron enhancement due to heating with a ~kJ short-pulse laser has been demonstrated in the integrated experiments at Osaka and Rochester. The neutron yields are being analyzed by comparing the experimental results to simulations. The details of the fast electron beam transport and the electron energy deposition in the imploded fuel plasma are complicated and further studies are imperative. The hydrodynamics of the implosion was studied including the interaction of the imploded core plasma with the cone tip. Theoretical works are presented on the hydrodynamics of a high-gain target for a fast ignition point design.

1. Introduction

Fast Ignition (FI) is a new scheme for inertial confinement fusion, in which a high-power short-pulse laser is injected in the imploded shell to heat and ignite the fuel core plasma [1-3]. Since its initial proposals, many theoretical, simulation, and experimental researches have been performed as described elsewhere in this special issue of Nuclear Fusion. Among those, fundamental processes such as high-intensity short-pulse laser interaction and hot electron physics, integrated experiments and the integrated design of the FI target are of great importance.

The role of FI integrated experiments that include an implosion with a drive laser and the heating of the imploded fuel with a separate short-pulse, high-power laser, is to examine the whole concept of the FI scheme and to demonstrate fast electron heating of the fuel plasma. There are several key physics to investigate in the FI integrated experiments such as laser interaction in the cone or laser-hole boring, hot electron generation, transport, and energy deposition in the fuel plasma, fuel heating and its scaling, nonuniform implosion of a shell target with a cone, and core-cone interactions. Conventional fundamental experiments by using plane targets are not always effective, since the complicated plasma environment in the integrated experiments cannot be reproduced with such simple plane targets, and the complexity of the FI target plasma often plays important roles. Detailed investigation of such physics processes is essential in FI research.

An FI integrated experiment was first performed at the Institute of Laser Engineering (ILE), Osaka University in 1998 by using Gekko-XII laser (λ=0.53 μm) for the implosion and a 100-TW class (PWM) short-pulse laser (1.053 μm) for heating. An enhancement of the neutron yield from the heated fuel was observed [4]. Then, the PWM laser was upgraded to a PW class laser in 2001, and a further neutron enhancement was achieved [5]. Based on these successful results, the FIREX-1 project [6] has been started in 2004. Its goal is to demonstrate fuel heating up to 5 keV by using the upgraded heating laser beams. For this purpose, LFEX laser (1.053 μm), which can deliver, at its full spec, an energy of up to10 kJ in a 0.5-20 ps pulse, has been constructed beside the Gekko-XII laser system. It has been activated and became operational since 2009, and upgraded integrated FI experiments have been started. On the other hand, the OMEGA-EP laser (1.053 μm) was constructed in 2008 at the Laboratory for Laser Energetics (LLE), University of Rochester [7]. It is specified to

deliver 2.6 kJ in a 10-ps pulse, and has been used for FI integrated experiments as a heating laser together with the 30-kJ OMEGA laser (0.35 μm) for the implosion. A neutron enhancement was observed in the FI integrated experiment with a ~1 kJ, 10-ps heating pulse [8]. The OMEGA laser has also been used for FI core assembly experiments [9]. These two facilities are currently the major sites where the FI integrated experiments are ongoing.

In this article, we describe the FI integrated experiments and simulations performed so far in Osaka with Gekko-XII and PWM/PW/LFEX lasers (ch. 2), those in Rochester with OMEGA and OMEGA-EP lasers (Ch. 3 & 4), as well as the ignition point design of FI target (ch. 5).

2. FI Integrated experiments and simulations at Osaka

Integrated experiments of FI targets were started in 1998 at ILE, Osaka, by using the Gekko-XII laser for implosion of a shell target and the PWM (PetaWatt Module) laser [10] injected through a hollow cone attached to the shell [4]. The PWM laser was a 100-TW class Nd:glass laser (λ=1.053 μm) with CPA (chirped pulse amplification) technology [11], and was constructed beside the Gekko-XII laser for high-intensity laser-matter interaction experiments.

The original concept of FI heating used the so-called hole-boring concept to ensure a clear path for the heating laser beam to the compressed core plasma [3]. Potential problems with this approach are propagation losses and deflection of the ultra-intense laser pulse in the plasma surrounding the highly compressed plasma, and the transport of the relativistic electron beam through a substantial length of the plasma. To mitigate this, a new scheme was introduced by inserting a hollow cone in a shell target. The cone is designed to keep the propagation path of the short-pulse laser free from plasma that forms around the imploding shell, thereby completely avoiding laser propagation issues.

A deuterated polystyrene (CD) shell, 500 μm in diameter and 7 μm in wall thickness, was irradiated with 9 beams among 12 of Gekko-XII laser. The total energy was 1.2 kJ in a 1-ns pulse. The cone was made out of gold with an opening angle of 60 degrees, and the distance from the tip to the center of the shell was 50 μm. At the moment of the maximum compression of the shell, the PWM laser was injected in the cone. The beam energy was 60 J in a 0.6 ps pulse. The beam was focused with an F/3.4

parabolic mirror onto the interior tip (bottom) of the cone.

D-D neutron yield was measured with plastic scintillators coupled to photomultiplier tubes. The neutron yield in the shot with the heating laser was increased by a factor of 10-30 to (1-3) x 10^5 from 1 x 10^4 without the heating laser. X-ray images were recorded with x-ray framing cameras. The density profile of the imploded core plasma was estimated from x-ray-backlit framing images assuming the residual mass of the shell at the maximum compression so that the peak density was 50-70 g/cm^3 and the diameter was 40-45 μm. Escaping hot electrons that were generated by the irradiation of the heating laser were measured with electron spectrometers. The temperature of the hot electron beam was 2-3 MeV, and the energy was 18-24 J, representing 30-40% of the heating laser energy.

Then the heating laser was upgraded in 2001 to a PW (Petawatt) laser. Similar experiments were performed with this upgraded heating laser [5]. Gekko-XII laser was operated at 2.5 kJ in a 1.2-ns pulse. Similar targets were used as before. The neutron yield was enhanced by three orders of magnitude from (2-5) x 10^4 with no short-pulse laser to 3 x 10^7 when the 0.5 PW (300 J, 0.6 ps) laser pulse was injected. The ion temperature of the heated plasma was estimated to be 0.8 keV from the neutron time-of-flight spectrum, which indicates that the temperature was doubled by the short-pulse beam. Heating took only place when the short-pulse laser was injected within ±50 ps around maximum compression.

Based on the successful result of fast heating with 100-TW- and PW-class lasers, upgraded experiments, the FIREX-1 project, was planned and started since 2003 at the ILE, Osaka [6]. Its goal is to demonstrate fuel heating up to 5 keV with a 10-PW class new heating laser, LFEX. LFEX is a Nd:glass-based 1.053-μm four-beam laser system. Its final output will be 10 kJ in a 0.5 - 20 ps pulse. The full system has four 37x37 cm square beams. A pulse from the oscillator is spectrally chirped and is amplified in a three-stage OPCPA (optical parametric chirped pulse amplification) system, rod amplifiers, and four-pass large-aperture disk amplifiers, which have been constructed beside the Gekko-XII laser, as shown in Fig. 1(left). The pulse is then compressed with a large grating pulse-compression system down to 1 ps. The beams are focused with an off-axis parabolic mirror (f = 4000 mm). The pulse compression and focusing system is constructed within two large vacuum chambers coupled with each other located near the interaction chamber of Gekko-XII as shown in Fig. 1(right).

Beam synchronization of LFEX to Gekko-XII is performed optically by using a common oscillator pulse for both lasers.

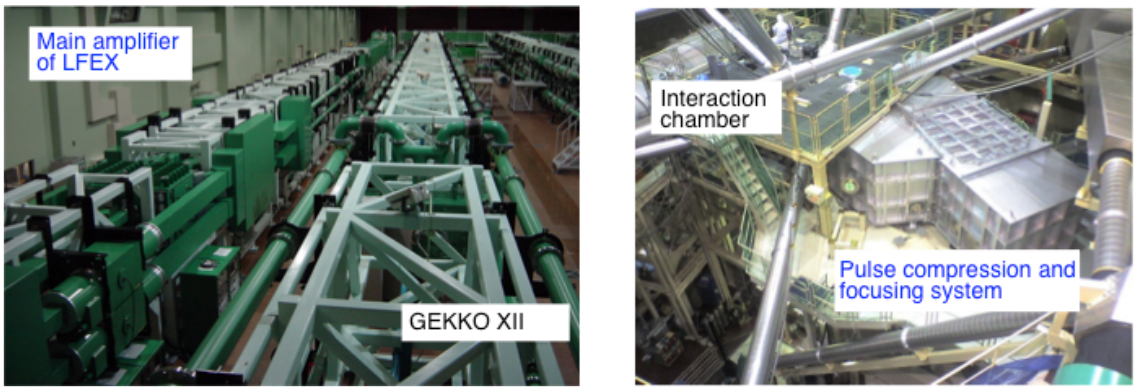

Fig. 1. (left) Gekko-XII laser system for implosion of the fuel target, and LFEX laser beam line for FI heating. (right) Pulse compression and focusing system with optics inside the vacuum chambers, and the interaction chamber.

One beam among four was activated in 2009, and the second beam in 2010. The compressed pulse width for one beam was 1.2 ps and the other was 1.3 ps. When two beams were overlapped, it was 1.5 ps. The contrast ratio was substantially improved in 2010. Saturable absorbers and AOPF (amplified optical parametric fluorescence) quenchers [12] were introduced to the OPCPA stages to reduce the prepulse level down to a contrast of 10^{-8}, defined as the power of the prepulse to the power of the main pulse. The beam focal spot size was estimated from x-ray images of planar targets irradiated by LFEX beams. A focal spot of 30-60 μm in diameter was observed resulting in an irradiation intensity of order of $1x10^{19}$ W/cm^2 on target. The spot size was the same for one beam and two beams that overlapped on the target. We limited the output energy to 700 J/beam for a 1 ps pulse duration to avoid damaging the optics, particularly the compressor gratings.

Implosion and heating experiments of FI targets for FIREX-1 have been performed by operating both Gekko-XII and LFEX lasers. Typical laser and target parameters were as follows. Gekko-XII laser for implosion: 0.53-μm light with an energy of 1.5-4.5 kJ in a 1.5 ns nearly Gaussian pulse in 2009, and a nearly flat-top pulse since 2010 using nine beams out of twelve. LFEX laser for heating: 1.053-μm light with an energy up to 1-2 kJ in 1-5 ps. The beam(s) were focused and injected into a cone attached to a shell target. CD shell targets: 500 μm in diameter and 7 μm in

thickness. A 10-20 μm wall-thickness Au cone with an opening angle of 30 or 45 degrees. Outer surface of the Au cone was coated with 10-μm-thick CH layer. The distance from the center of the shell to the cone tip was 50 μm.

Figure 2 shows the measured neutron yield obtained from heating the imploded fuel by a 0.6 ps PW laser in 2002 [5], 1 ps and 5 ps LFEX beam in 2009, and 1.5 ps LFEX in 2010 [13, 14]. The neutron yield without heating beam was $1x10^4$ in 2009 experiments, and $1x10^6$ in 2010 experiment. The difference is due to different pulse shapes of the Gekko-XII laser for imploding the shell. In the 2009 experiment, an enhancement of the neutron yield was achieved by 1 ps and 5 ps pulses. A 30-degree cone was used for the 5 ps data, while a 45-degree cone was used for 1 ps data. Although the result looks as if there is a strong dependence on the pulse width, it is not clear because other experimental conditions were not the same.

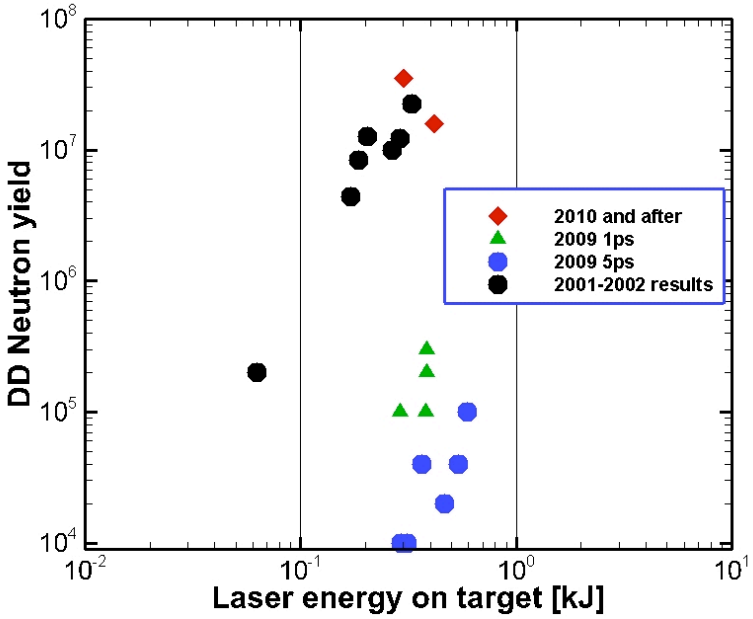

Fig. 2. The measured neutron yield obtained in the various ILE experiments as a function of the short pulse laser energy in 2010 (diamonds), 2009 (blue circles and green triangles), and 2001-2002 (black circles) as described in the text.

Hot electrons that escaped the target were measured in 2009 and had an energy spectrum of about 10 MeV. This was higher than expected. Efficient energy deposition in the present level of the expected fuel ρR = 100-300 mg/cm^2 requires electrons of a few MeV. According to a separate measurement of the preformed plasma and

simulation analyses, the high electron energies were attributed to the preformed long-scale-length plasma created by a prepulse in the LFEX beam in the cone. The prepulse level was significantly reduced in 2010 to improve the heating efficiency. The estimated contrast was of order of 10^{-4} in 2009 and 10^{-8} in 2010.

In the 2010 experiment, we have measured a neutron enhancement of up to 3.5×10^{7} with total heating energy of 300 J on target, which is higher than the yield obtained in 2009 experiment and exceeded the previous data in 2002. The neutron enhancement was only observed when the heating laser was injected within 50 ps around the time of the maximum x-ray emission from the core. The estimated ion temperature is ~ 0.8 keV.

Numerical simulations play an important role in FI studies. However, the time and space scales in FI simulations vary widely from the initial laser irradiation for the implosion, to the relativistic laser plasma interaction and the final fusion burning. All the physical processes are desired to be self-consistently described in a numerical calculation. However, it is a formidable task to simulate relativistic laser plasma interaction and radiation hydrodynamics in a single computational code. At ILE and the National Institute for Fusion Science (NIFS), an integrated simulation system, "Fast Ignition Integrated Interconnecting code" (FI^3) [15, 16] was developed for the purpose. It consists of a collective Particle-in-Cell (PIC) code [17], a Relativistic Fokker-Planck and hydrodynamic code (RFP-hydro) [18,19], and a radiation hydrodynamics code [20-22].

These integrated simulations indicate that the heating efficiency is very sensitive to the preformed plasma due to the pre-pulse of the heating laser [23]. Relevant to the fast electron generation in the heating process, the dependence of the fast electron slope temperature on the preformed plasma scale length λ_p is investigated using PIC simulations. In the typical FIREX-I condition, T_h are evaluated 3.2 MeV, 6.2 MeV and 11.2 MeV for λ_p =1 μm (w/o preformed plasma case), 3 μm, and 10 μm respectively. In order to obtain the core heating property, a RFP-hydro simulation is carried out using the hot electron distributions obtained by PIC simulation. The conversion efficiency from the heating laser to fast electrons was estimated to be 48% without preformed plasma in the cone (39% to electrons less than 10 MeV) and the transport efficiency of the fast electrons to the core was calculated with 16%, resulting in a total coupling efficiency of about 8%. With preformed plasma the coupling

efficiency drops to 4.7% and 1.7% for λ_p =3 μm and 10 μm, respectively. However, it is yet difficult to discuss in detail the heating process, because there are many unknown factors in the electron beam parameters as well as in the heating models. The assembled plasma in front of the cone tip is highly inhomogeneous in density and temperature (see for example Fig. 5), and this will greatly affect the number of generated neutrons. Spatial profile of the heating, such as a filamentary structure for example, may cause similar results. Inferring a coupling efficiency from the measured neutron number is difficult because it depends on the details of the compressed plasma and the heating. Energy deposition in hotter parts of the plasma generates significantly more neutrons than if the same amount of energy is deposited in colder parts of the fuel. In addition, there could be other mechanisms such as shock heating from a decompressing cone into the fuel assembly that might contribute to the neutron production. Therefore further investigations of the fuel assembly and of each process of FI heating are needed to gain a better understanding of the energy deposition.

Several new target designs are proposed or confirmed through the FI^3 simulations to improve the heating efficiency. Double cone target [24,25], a low-Z pointed cone target [23,26,27], self-magnetic field generation due to the resistive gradient[26] or implosion dynamics [28], and external magnetic field [29]. Their main purpose is to collimate the fast electron beam. For example, using a double cone target, fast electrons which escape from the cone side wall are confined toward the forward direction by electrostatic and quasi-static magnetic fields. Some designs have been already realized in practice.

3. OMEGA integrated FI experiments and simulation

This section summarizes integrated fast-ignition experiments on the OMEGA Laser Facility [31] and hydrodynamic simulations relevant to the cone-in-shell implosions. The integrated experiments produced up to ~1.4×10^7 additional neutrons with a 1 kJ, 10-ps short-pulse laser [8]. The targets were 40-μm thick, ~870-μm-outer-diameter CD shells with an inserted hollow gold cone. The cone had an inner full opening angle of 34° and a small circular flat disc in the tip with a wall thickness of 15 μm. Details and pictures of the target design can be found in reference [8]. The shells were imploded with 54 out of the 60 UV OMEGA beams with energy of ~18 kJ in a 2.7 ns pulse. The 1053-nm-wavelength short pulse from the OMEGA EP

laser had an energy of ~1 kJ and a 10-ps duration and was focused to a spot with a radius of R_{80} = (26±2) μm containing 80% of the laser energy with an average intensity of ~4 × 10^{18} W/cm^2. A nanosecond prepulse with energy of ~22 mJ preceded the OMEGA EP pulse that caused significant pre-plasma formation inside the cone.

The main diagnostic that measured the yield of thermonuclear neutrons was a liquid-scintillator time-of-flight detector that was especially hardened against the strong x-ray background generated in the integrated experiments [32]. The liquid scintillator detector completely suppressed the background at the time when the 2.45-MeV neutrons arrived and provided reliable neutron-yield data. Examples of the measured neutron spectra are shown in Fig. 3 for different timings and two target types. The spectrum for an early arrival (3.52 ns) of the short-pulse laser is very similar to spectra obtained without short-pulse laser. The spectrum at a later time (3.62 ns) for a 10 μm flat tip shows a significant enhanced neutron signal, while the increase is not as pronounced for the 40 μm flat tip (3.65 ns). No attempt was made to extract an ion temperature from the noisy and broadened spectra. The implosion without the short-pulse produces thermonuclear neutrons in the hot, dense core surrounded by the cold shell as well as in the corona of the plasma since the whole shell was deuterated and the drive laser heats the region between the critical and the ablation surface to temperatures >1 keV. The corona yield (~0.7 × 10^7) was treated as an offset and was subtracted from the measured yields.

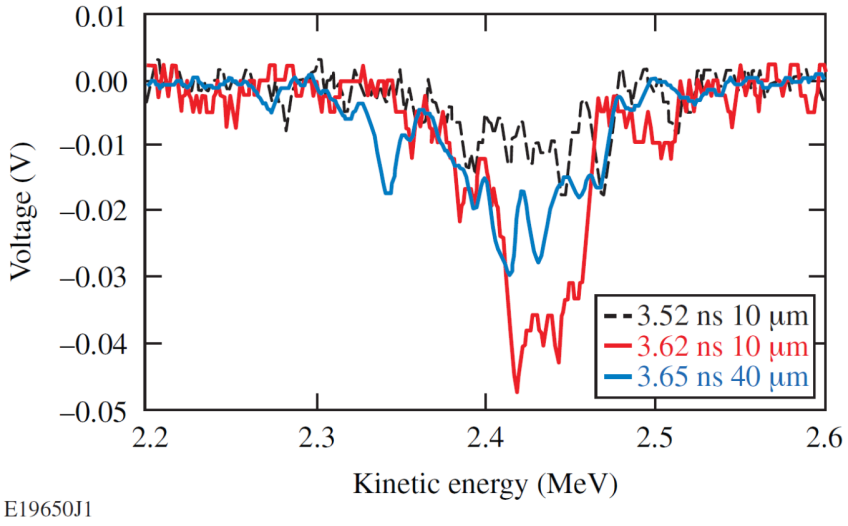

Fig. 3: Time-of-flight spectra of 2.45 MeV thermonuclear neutrons from OMEGA integrated fast-ignition experiments. Spectra with various timings of the OMEGA EP

beam are shown for two target types [8]. Reproduced with kind permission of the American Institute of Physics.

Figure 4 shows the measured neutron yield as a function of the arrival time of the OMEGA EP pulse in the cone. Two types of targets were used. The red circles show the results for a 10-μm tip diameter and the blue triangles for a larger tip (40 μm). The 10 μm data show a peak in neutron yield at a delay time of 3.65±0.02 ns. The dashed curve is a fit of a Gaussian profile to the red circles. The gray bar shows the yield without the short-pulse beam. The 10-μm data show an enhancement in neutron yield by a factor of ~4 for the smaller-tip targets and a properly timed short-pulse beam. The $(1.4\pm0.6) \times 10^7$ additional neutrons resulted from heating by the short-pulse laser in a narrow time window of less than 100 ps. It is not yet clear why the larger tip targets produced a lower yield. Hydrodynamic simulations indicate that both targets behave very similarly during the implosion. It is therefore likely that the lower neutron yield is related to the short-pulse interaction physics. Possible causes might be that a smaller tip leads to a better electron transport. Intense laser-plasma interaction with the side wall of the cone might lead to higher conversion efficiency into fast electrons [33] and enhanced surface acceleration of fast electrons [34]. But the measurements could also point to that other mechanisms might be responsible for the neutron yield enhancement than direct fast electron deposition in the compressed CD. The smaller tip target contains less amount of gold material in the cone tip. Simulations show a strong heating of the cone tip by the short pulse laser. A smaller tip could be heated to a higher temperature than the larger tip target for a constant conversion efficiency of laser energy into fast electrons, setting up a strong shock wave that could generate additional thermonuclear neutrons while expanding into the compressed CD.

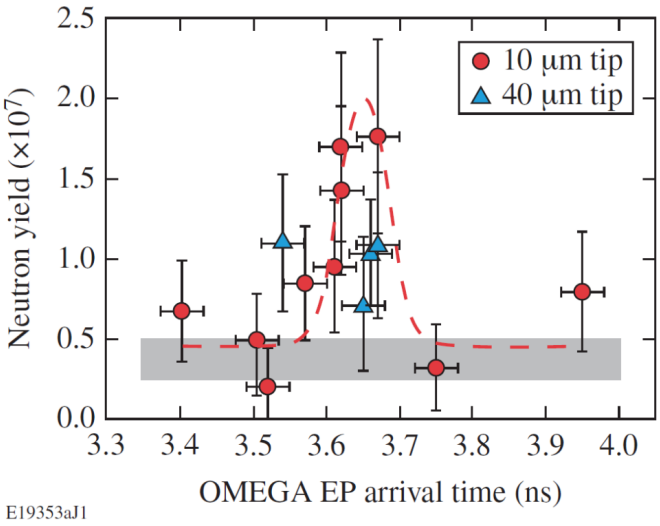

Figure 4: Neutron yield as a function of the arrival time of the short-pulse laser for 10-μm (circles) and 40-μm (triangles) tip diameter cone targets. The gray area represents data without the short-pulse laser [8]. Reproduced with kind permission of the American Institute of Physics.

Fast electrons that escaped the target were measured in two different directions with electron spectrometers. Slope temperatures of around 3 MeV were inferred from the spectra in the direction along the short pulse laser and in a direction almost perpendicular to the cone axis. The temperatures are significantly higher than that expected based on ponderomotive scaling of the average laser intensity in vacuum. The higher electron energies may be caused by cone filling by preformed plasma. Two-dimensional hydrodynamic simulations show that the nonrelativistic critical density shifted by ~100 μm away from the original inner cone wall position at the time when the main short pulse interacted. Recent two-dimensional PIC simulations [35] studied the fast electron generation by an intense short pulse in the preformed plasma. The PIC simulations used the initial plasma density profile from the hydrodynamic simulations that included the preformed plasma inside the gold cone. The electron generation from the laser interactions with the preformed plasma and the electron transport was studied for densities up to 100 times of the critical density and for times of up to ~7 ps. The simulation results showed a large mean divergence half angle of 68 degree of the forward transported electrons and electron spectra with slope temperatures that are very similar to the measured spectra. The simulations demonstrated that the

stochastic fast electron generation mechanism is responsible for the relatively high fast electron energy.

The implosion of cone-in-shell targets in the integrated experiments on OMEGA was modeled using the radiation-hydrodynamic code DRACO [36]. The simulations used 2-D cylindrically symmetric geometry, Eulerian hydrodynamics, included radiation transport and 3-D laser ray trace, and accounted for the reduction in hydrodynamic efficiency because of laser cross-beam energy transfer. Figure 5 shows the target density and temperature distributions in the simulation for a 10-μm-diameter cone tip at 3.65 ns, when the maximum neutron yield increase was observed in the joined shots. The target is not fully compressed at this time, with the maximum density of ~12 g/cm^3 and the areal density of ~100 mg/cm^2 in the direction perpendicular to the cone axis from the center of the hot spot. The time of shock wave break out through the cone tip is 3.71 ns in the simulation, which is in good agreement with the measured value of 3.72 ± 0.03 ns in the experiment [8]. The peak in the neutron yield increase in the joined shots is, therefore, observed slightly before the cone tip break out. The tip break out can explain a lower coupling of the OMEGA-EP pulse energy with the plastic core at later times when the cone fills up quickly with the implosion plasma. The peak compression is achieved later in the simulation, at 4 ns, when the compressed density reaches 100 g/cm^3 and the areal density is about 450 mg/cm^2.

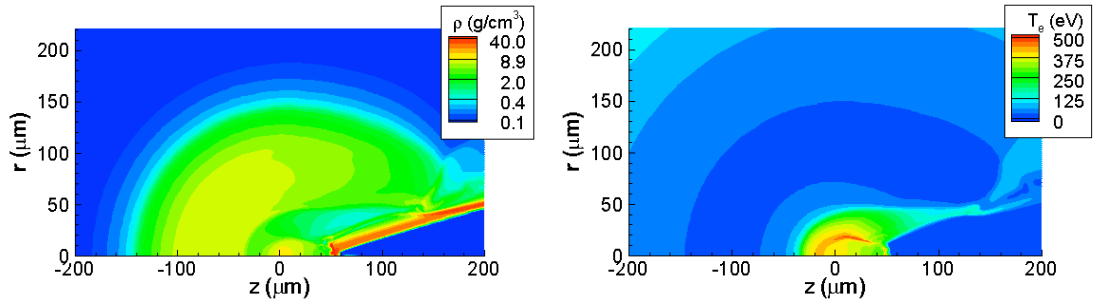

Fig. 5: DRACO simulation of cone-in-shell target implosion in the OMEGA experiments. (a) Plasma density, (b) electron temperature at the time 3.65 ns, when the neutron yield increase is maximum in the joined shots.

Ways to improve performance of cone-in-shell targets in the integrated experiments include reduction of the OMEGA-EP prepulse energy, which will reduce the distance between the region where the fast electrons are generated and the

compressed core. Improvements in the OMEGA-EP focal spot quality and energy increase will boost the laser intensity and the total short-pulse energy coupled to the core. Using targets with cone tips made of lower-Z materials can reduce the scattering losses of fast electrons and allow using thicker tips that are more resistant to the high implosion pressure. A slight implosion asymmetry introduced by an enhanced laser drive or a reduced shell radius from the cone side can also reduce the pressure on the cone tip and delay the tip break out time to be closer to the peak compression time [37].

4. Core assembly and core-cone interaction experiment at OMEGA

Before the integrated experiments were started at Rochester with OMEGA-EP, a series of experiments on the hydrodynamics of cone-attached shell targets were performed on the OMEGA laser, as part of a US-Japan joint research in 2003-2004 [38]. The hydrodynamics of cone-in-shell targets were investigated in many aspects such as the non-uniformly imploded core density, the core dynamics, the core-cone interaction, the cone dynamics, the preheat level of the cone tip, the misalignment of the cone axis, and the contamination of the fuel by the cone material. Among those, particularly, an important result was obtained on the core-cone interaction.

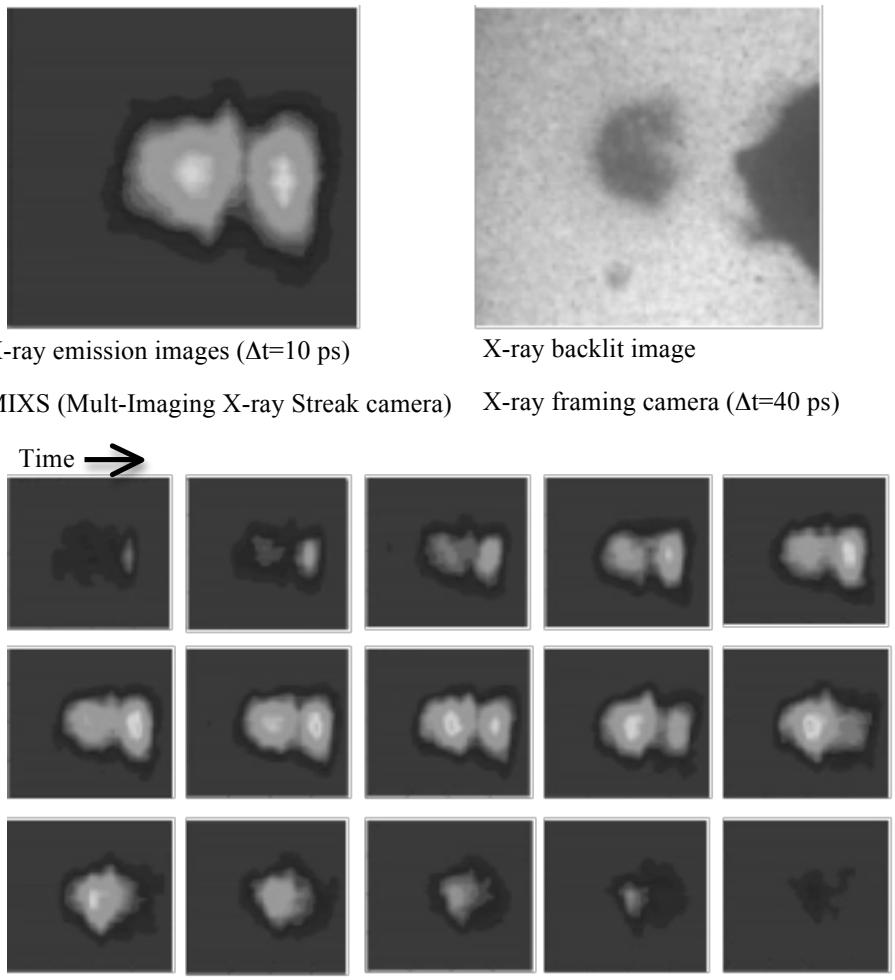

Fig. 6 Framing images of x-ray self emission observed by MIXS (top left and bottom) and x-ray backlighting by x-ray framing camera (top right). Frame interval in the bottom pictures is 40 ps. The field of view of each image is 200 μm x 200 μm. (after Ref. [38])

The experiment was performed with an energy of 15 kJ in a 1 ns pulse and 35 beams of the OMEGA laser (λ=0.35 μm) for implosion. The target was a plastic shell with a diameter of 1000 μm and a wall thickness of 25 μm. Some of the shells contained 5 atm D_2 or D-^{3}He gas for diagnostic purposes, and some others had no gas. The core and the cone dynamics were observed with time-resolved x-ray framing imaging. Self-emission images (> 2 keV) were recorded with the MIXS (multi-channel X-ray streak camera with image sampling procedure to obtain two-dimensional time resolved images) [39]. The exposure time of each frame was 13 ps. X-ray backlit images were recorded with x-ray framing camera by using x-rays emitted from

separately produced V (5.5 keV) or Fe (7 keV) plasmas [40]. Fig. 6 shows the data. The MIXS camera provides a "movie" that complements the backlit images to give a vivid visual impression of what the implosion, jet, and cone look like; where the emission comes from; and how the fuel assembly evolves with time. One can clearly see that the X-ray emission comes from the tip of the cone first, and then the imploded core is formed. The core is not moving, and its shape is not spherical but like a jellyfish, with a cutout in the direction of the cone, and changing in time. From a comparison with 2-D simulations, it is found that this early X-ray emission from the cone is due to a shock wave propagating in the deuterium plasma inside the shell, which leads a jet from the center of the core toward the cone. Then, the shell plasma converges and forms the core afterward. Such a precursor shock wave toward the cone has the ability to degrade the cone quality before the heating beam is injected. The effect of the jet on the cone tip is also clearly seen in the x-ray backlit images. When the target had no gas fill, the early emission from the tip of the cone was found to be very weak, which indicates that the shock wave from the core was much weaker. It is of great importance to investigate such hydrodynamics in detail for FI research, since these phenomena need to be carefully considered in the target design.

5. Ignition point design and hydrodynamics of FI targets

The original FI scheme had three steps: fuel assembly with direct or indirect drive; a hole-boring step in which a high intensity laser evacuates a path through the coronal plasma (produced in the first step) with ponderomotive and thermal pressure; and finally, a very intense short pulse laser heats the fuel to ignition. Although some effort continues in modeling and experiments of this hole-boring approach, most current effort studies an approach using a cone embedded in the fuel capsule. This choice was made because the hole-boring scheme would require too much laser energy to drill the hole. Experiments with cones and their pre-made laser path could begin to study energy coupling to the compressed fuel much earlier.

Although fuel assemblies for FI are not required to reach the high densities required for central hotspot ignition and are less sensitive to hydrodynamic instabilities than those for hotspot ignition, FI assemblies have constraints that central ignition assemblies don't: the distance between the assembled fuel and the critical surface must

be minimized. If the electron beam has an angular distribution with FWHM of order 120^o as suggested by PIC simulations, and there is no beam confinement by, for example, magnetic fields, the coupling efficiency will be significantly reduced for standoff distances comparable to the beam diameter. The practical column density (including multiple scattering) between the critical surface and the compressed fuel should be less than a stopping range and much less than a stopping range if beam is composed of 1-3 MeV electrons. The volume of the central low density fuel region should be minimized in order to maximize the fuel column density for a given compressional energy. A small hotspot provides more tamping while the shell heated by the electron beam is heating and disassembling.

Capsule designs for cone-in-shell implosions begin with symmetric shell-only implosions. There have been two solutions to the problem of producing a fuel assembly with small or vanishing central hotspot in the symmetric 1D approximation. The first design is based on a self-similar solution [41] that takes a shell with density and velocity gradients into a uniform stagnated system that is both isobaric and isentropic and hence isochoric. A similar solution that took a uniform sphere into a compressed uniform sphere was shown by Moreeuw and Saillard [42]. In their design, the reflected shock from the center stagnates the incoming shell and final drive shock, much like the shock ignition scheme but without the central adiabat jump. The transition from a fuel shell of uniform density to a shell required by the self-similar solution with the proper density and velocity gradients is accomplished by a single shock and rarefaction [43].

A typical laser pulse shape for direct drive together with a diagram of the driven capsule is shown in Figure 7. These pulse shapes deliver much of their energy at the end of the pulse at high intensity. Therefore, high efficiency requires zooming. Because the implosion velocity ($6x10^6$ cm/s) for these designs is low (the specific energy in optimized FI assemblies is much lower than those for central hotspot ignition), this high peak power leads to low rocket efficiency. Nevertheless, this scheme leads to high column density for a given delivered energy. For the design shown in Figure 7, 485 kJ of laser energy produced 2.4 g/cm^2 column density and an approximately uniform central density of 450 mg/cm^3 from a fuel mass of 0.9 mg.

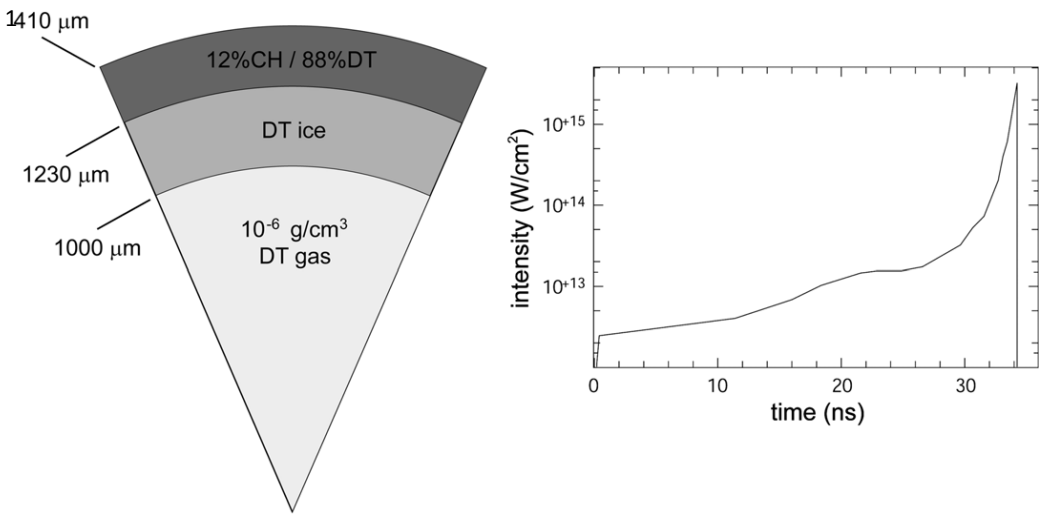

Fig. 7. Capsule build and laser intensity for directly driven capsule that forms an isochoric fuel assembly.

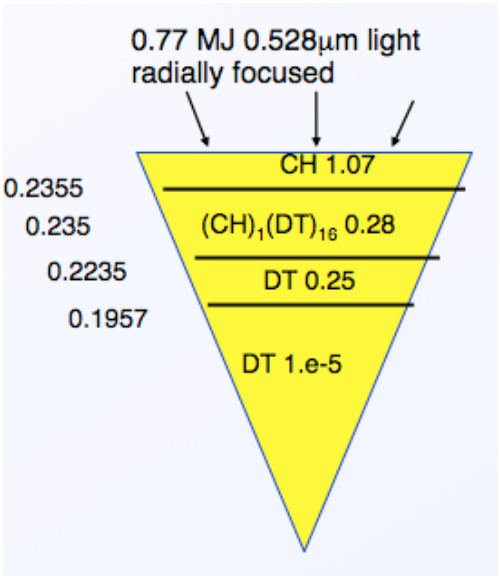

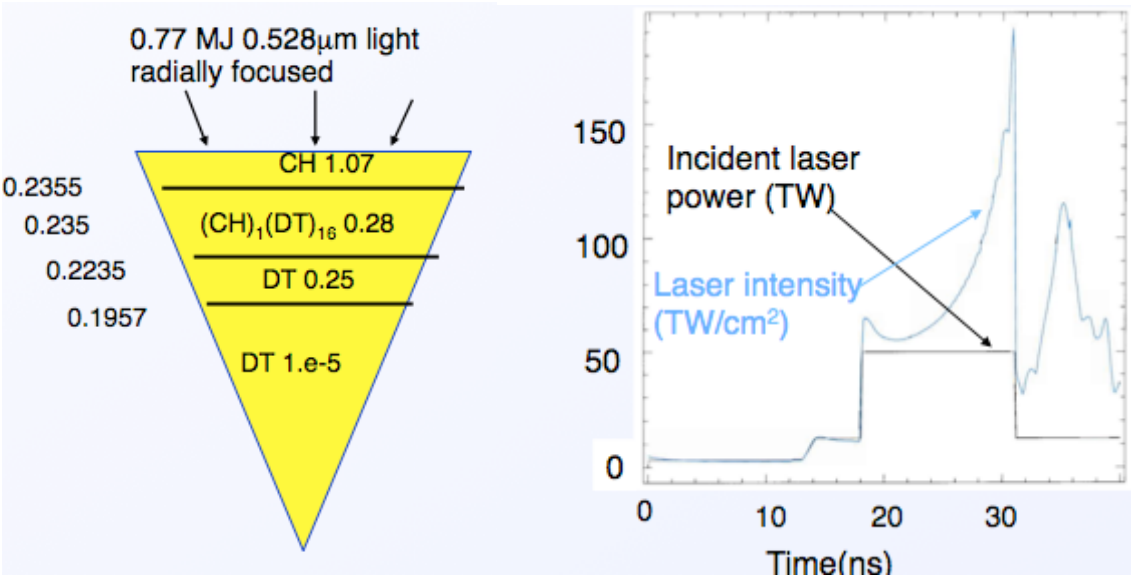

Fig. 8. a) Capsule build for conventionally pulse-shaped implosion for FI
b) Conventional pulse shape for directly driven target

A more conventional implosion design [44] uses a sequence of shocks or a sequence of pickets and shocks (for adiabat shaped designs) much like pulse shapes used for conventional hotspot ignition. The difference lies in that the FI implosions drive more mass for a given laser energy. Figure 8 shows such a design together with the laser pulse that drives it [45]. The peak intensity is quite high because the laser is assumed to radially incident.This design yields a column density of 2.9 g/cm^2 for fuel mass 4 mg and 770 kJ laser energy radially incident. Because the implosion velocities are low, targets optimized for rocket efficient are driven with low intensity (of order 10^{14} W/cm^2 with 1/3 μm light) while implosions chosen to minimize Rayleigh-Taylor instabilities are driven at 10^{15} W/cm^2. These choices differ in coupling efficiency by about a factor of 2.

The thickness of the cone wall is set by the requirement that the implosion does not collapse the cone or fill it with even critical density plasma. The cone is driven by the ablation pressure driving the capsule, the pressure in the capsule increases due to convergence as the shells kinetic energy is converted into compressional energy near the end of the implosion as well as ablation pressure as the radiation or laser light interacts with the cone material. For ignition or high gain designs, these requirements lead to cone thicknesses exceeding 100 microns of gold near the initial shell radius,

tapering to a few tens of microns near the cone tip. If the cone is composed of a lower density material, the thickness will need to be increased. Increasing the thickness near the cone tip, increases the outer radius of the cone tip and hence the axial position where ballistic fuel elements reach the symmetry axis.

When the fuel stagnates it comes to a pressure large compared to the ablation pressure. For a Fermi-degenerate deuterium-tritium mixture, this pressure is: $\mathrm{Pr}_{abla}(Mbar) = 2.3\rho^{5/3}(g/cm^3)$. For 1000 g/cm^3 density, the pressure is 230 Gbar. This can clearly disrupt the cone tip. This stagnation pressure is balanced by the ram pressure of the incoming fuel in all directions except in the direction of the cone tip, where there is no incoming fuel. This produces a jet (or one-dimensional rarefaction), driven with the stagnation pressure and pointing directly at the cone tip. The velocity of this jet is given by the sound speed in the compressed fuel. Thickening the cone tip will make little difference on the propagation of this jet into cone until the density in the rarefaction has dropped to that of the cone.

The deformation of the cone tip increases the distance between the critical surface and the fuel. If the shock, driven by the jet, breaks out of the cone tip, another rarefaction, traveling at about three times the shock speed, is launched into the cone void. If the cone tip column density is increased to avoid this problem, the tip material will cause multiple scattering and energy loss of the incoming electron beam. For this reason, the tip is often selected from lower atomic number materials, like carbon or aluminum. This tip can be sheathed in higher density, higher atomic number materials in order to minimize the tip radius.

The time available for these jets to cause their mischief is given by the time between initial fuel stagnation, when the leading edge of the fuel shell comes to stagnation pressure, to the time of full fuel assembly. This time scales as the shell thickness after convergence effects have thickened the shell divided by the implosion velocity. For ignition or high gain designs, this time is of order 1 ns, leading to separation distances of 100-200 μm.

Increasing the time for the jet to reach the cone tip compared to the stagnation time also protects the cone tip. Increasing the separation between the center of the

implosion and the cone tip accomplishes this. An additional benefit of this procedure is to improve the quality of the implosion because the perturbation due to the cone covers a smaller solid angle. This increase in fuel-critical surface distance can be part of an optimization that includes increasing the cone tip thickness.

Asymmetric implosions can also increase the jet arrival delay. For example, consider a shell of uniform thickness but distorted so that its inner radius on the cone side is closer to the center of convergence than the shell directly opposed to the cone. The near side shell will arrive at the center of convergence, but won't stagnate because the opposite side has not arrived yet. It will continue past the center and stagnate when the opposite side arrives. However, by this time the near side fuel has fully assembled on axis so the reflected shock serves only to compress this fuel further. No jet is launched. Preliminary calculations using a scheme of this sort produced a dense fuel-critical surface separation of about 50 μm [46].

For radiation driven systems (and to a substantially smaller degree for directly driven systems), radiation produced in the laser-hohlraum (laser-ablator) interaction can penetrate the capsule shell and couple to the cone. Hard radiation (m-band or l-band) produced at the hohlraum wall can penetrate the capsule and efficiently couple to a high atomic number cone. A thin layer from this cone can then blow off into the path of the incoming shell. In simple one dimensional test problems, this high-Z blowoff can extend for more than 100 μm from the high atomic number surface. This material impedes the implosion around the cone and can possibly mix with the fuel. At this time, no simulations have yet been performed to assess mixing.

There have been several proposed solutions to this problem. Here, we sketch some of these schemes and possible drawbacks. Tamping the cone with low atomic number materials, that couple weakly to hard photons, restricts the high-Z expansion to a few tens of microns. If the cone is made entirely from a low-Z material like diamond, the cone won't blow off. However, the lower density (compared to gold) requires a thicker cone. The implosion will assemble farther from cone tip and more energy will be lost from the implosion to do PdV work compressing the cone.

Adding high-Z or mid-Z dopants to the ablator will absorb these penetrating photons before they reach the cone. Hydrodynamic stability requirements limit the concentration of these dopants in the ablator because abrupt changes in density are classically unstable. The dopant provides increased opacity not only for the hard

photons, but also for photons near the Planckian peak that produce the ablation pressure. This leads to reduced implosion efficiency. The self-similar implosion [41, 43] tolerates lower dopant levels than the more conventional one [44] because the peak intensity occurs later in the implosion when the shell column density has increased due to convergence. The rocket efficiency is increased at the expense of supplying the peak intensity when the capsule has smaller area to accept the radiation.

A parameter study of reactor scale cone-shell implosions [37] using gold cones with diamond tips 130 μm thick was performed using the radiation hydrodynamics code, HYDRA [47]. The symmetric 1-D design had 3 mg of DT fuel, absorbed 580 kJ of x-ray energy (consistent with 1.7-2.3 MJ of laser energy) and assembled to column density 2.8 g/cm^2. The radius and tilt of the diamond tip, cone offset from the center of convergence, and the variation of shell radius from cone side to far side were varied. The peak fuel density was about 250 g/cm^3, the peak column density (approximately in the radial direction) was 2.5 g/cm^2, while the column density about the peak density in the axial direction was about 1.7 g/cm^2. The compressed cone tip thickness was about 30 μm with column density 0.02-0.08 g/cm^2. The distance to the peak density from the cone tip was 100-140 μm, but the distance to half peak density was only 20-30 μm. So the total distance between the critical surface and peak density was about 150 μm, but only 50 μm to the beginning of the dense region. These distances are still so large that some guiding of electrons will be necessary to get good coupling efficiency.

6. Summary

Fast ignition integrated experiments have been performed with cone-in-shell targets with the Gekko-XII and LFEX lasers at ILE, Osaka, and the OMEGA and OMEGA-EP lasers at LLE, Rochester. Similar neutron enhancements of several 10^7 additional neutrons were produced by the short-pulse lasers. An estimation of the heating efficiency is difficult and depends on the details of the plasma parameters of the imploded fuel, the fast electron beam transport, and the electron energy deposition in the imploded fuel plasma. The processes are not yet well understood and further studies are required to study those aspects both in separate experiments as well as in integrated experiments. Although the experiments were at a rather low energy level, it is expected that FI becomes a candidate for an efficient ignition scheme of inertial fusion energy. A point design is underway to explore the possibility of ignition and fusion burn by FI.

Several schemes for assembling fuel with small central low density regions were described. The difficulties imposed by including a cone in the shell implosion were discussed. Target designs with adequate fuel target density exist, although the distance separating critical density and high density is currently so large that electron guiding is required for good coupling efficiency. Work is ongoing to address this issue. Prepared by LLNL under Contract DE-AC52-07NA27344.

References

[1] Yamanaka T 1983 (in Japanese, unpublished).

[2] Basov N G, Gus'kov S Yu, and Feoktistov L P 1992 J. Sov. Laser Res. **13** 396

[3] Tabak M, Hammer J, Glinsky M E, Kruer W L, Wilks S C, Woodworth J, Campbell E M, Perry M D, Mason R J 1994 Phys Plasmas **1** 1626

[4] Kodama R, Norreys P A, Mima K, Dangor A E, Evance R G, Fujita H, Kitagawa Y, Kurshelnick K, Miyakoshi T, Miyanaga N, *et al*. 2001 Nature **412** 798

[5] Kodama R, Shiraga H, Shigemori K, Toyama Y, Fujioka S, Azechi H, Fujita H, Habara H, Hall T, Izawa Y, *et al*. 2002 ibid, **418** 933

[6] Azechi H, Mima K, Fujimoto Y, Fujioka S, Homma H, Isobe M, Iwamoto A, Jitsuno T, Johzaki T, Kodama R, Koga M, Kondo K, Kawanaka J, Mito T, Miyanaga N, Motojima O, Murakami M, Nagatomo H, Nagai K, Nakai M, Nakamura T, Nishihara K, Nishimura H, Norimatsu T, Ozaki T, Sakagami H, Sakawa Y, Sarukura N, Shigemori K, Shimizu T, Shiraga H, Sunahara A, Taguchi T, Tanaka K A, Tsubakimoto K 2009, Nuclear Fusion **49** 104024

[7] Waxer L J *et al*. 2005 Opt. Photonics News **16** 30

[8] Theobald W, Solodov A A, Stoeckl C, Anderson K S, Betti R, Boehly T R, Craxton R S, Delettrez J A, Dorrer C, Frenje J A, Glebov V Yu, Habara H, Tanaka K A, Knauer J P, Marshall F J, Marshall K L, Meyerhofer D D, Nilson P M, Patel P K, Chen H, Sangster T C, Seka W, Sinenian N, Ma T, Beg F N, Giraldez E and Stephens R B 2011 Phys. Plasmas **18** 056305

[9] Stephens R B, Hatchett S P, Tabak M, Stoeckl C, Shiraga H, Fujioka S, Bonino S, Nikroo A, Petrasso R, Sangster T C, Smith J and Tanaka K A 2005 Phys. Plasmas **12** 056312

[10] Kato Y et al. 1997 "Fast ignition and related plasma physics issues with high-intensity lasers", Plasma Phys. Control. Fusion **39** 145

[11] Strickland D and Mourou G 1985 Opt. Commun. **56** 219

[12] Kondo K, Maeda H, Hama Y, Morita S, Zoubir A, Kodama R, Tanaka K A, Kitagawa Y and Izawa Y 2006 J. Opt. Soc. Am. B **23** 231

[13] Shiraga H, Fujioka S, Nakai M, Watari T, Nakamura H, Arikawa Y, Hosoda H, Nagai T, Koga M, Kikuchi H, Ishii Y, Sogo T, Shigemori K, Nishimura H, Zhang Z, Tanabe M, Ohira S, Fujii Y, Namimoto T, Sakawa Y, Maegawa O, Ozaki T, Tanaka K, Habara H, Iwawaki T, Shimada K, Nagatomo H, Johzaki T, Sunahara A, Murakami M, Sakagami H, Taguchi T, Norimatsu T, Homma H, Fujimoto Y, Iwamoto A, Miyanaga N, Kawanaka J, Jitsuno T, Nakata Y, Tsubakimoto K, Morio N, Kawasaki T, Sawai K, Tsuji K, Murakami H, Kanabe T, Kondo K, Sarukura N, Shimizu T, Mima K and Azechi H 2011 Plasma Phys. Control. Fusion **53** 124029

[14] Shiraga H, Fujioka S, Nakai M, Watari T, Nakamura H, Arikawa Y, Hosoda H, Nagai T, Koga M, Kikuchi H, Ishii Y, Sogo T, Shigemori K, Nishimura H, Zhang Z, Tanabe M., Ohira S, Fujii Y, Namimoto T, Sakawa Y, Maegawa O, Ozaki, Tanaka K A, Habara, Iwawaki T, Shimada K, Nagatomo H, Johzaki, Sunahara A, Murakami M, Sakagami H, Taguchi T, Norimatsu T, Homma H, Fujimoto Y, Iwamoto A, Miyanaga N, Kawanaka J, Jitsuno T, Nakata Y, Tsubakimoto K, Sueda K, Morio N, Matsuo S, Kawasaki T, Sawai K, Tsuji K, Murakami H, Kanabe T, Kondo K, Kodama R, Sarukura N, Shimizu T, Mima K, Azechi H 2012 High Energy Density Physics, **8** 227

[15] Nagatomo H, Johzaki T, Sakagami H, Mima K, Nakao Y, Taguchi T, Yokota T, Sunahara A, Nishihara K, and Izawa Y 2004 Proceedings of the International Atomic Energy Agency (IAEA) Fusion Energy Conference, Vilamoura, IAEA, Vienna, 2004, Paper No. IAEA-CN-116/IFP/07–29

[16] Sakagami H, Johzaki T, Nagatomo H and Mima K 2006 Laser Part. Beams **24** 191–8

[17] Sakagami H and Mima K 2004 Laser Part. Beams **22** 41–4

[18] Johzaki T, Nagatomo H, Sakagami H, Sentoku Y, Nakamura T, Mima K, Nakao Y and Yokota T 2006 J.Phys. IV **133** 385–9

[19] Yokota T, Nakao Y, Johzaki T and Mima K 2006 Phys.Plasmas **13** 022702

[20] Nagatomo H, Johzaki T, Sunahara A, Shiraga H, and Mima K 2006 J. Phys.IV **133** 397

[21] Nagatomo H, Johzaki T, Sunahara A and Mima K 2006 J. Plasma Phys. **72** 791

[22] Sunahara A, Sasaki A and Nishihara K 2008 J. Phys.: Conf. Ser. **112** 042048

[23] Johzaki T, Nagatomo H, Sunahara A, Cai H-B, Sakagami H, Nakao Y and Mima K 2011 Nuclear Fusion **51** 073022

[24] Nakamura T, Sakagami H, Johzaki T, Nagatomo H, Mima K and Koga J 2007 Phys. Plasmas **14** 103105

[25] Cai H-B, Mima K, Zhou W-M, Johzaki T, Nagatomo H, Sunahara A and Mason R J 2009 Phys. Rev. Lett. **102** 245001

[26] Johzaki T, Sentoku Y, Nagatomo H, Sakagami H, Nakao Y and Mima K 2009 Plasma Phys. Control. Fusion **51** 014002

[27] Sunahara A, Johzaki T, Nagatomo H, Mima K 2012 Laser and Particle Beams **30** 95-102

[28] Nagatomo H, Johzaki T, Sunahara A, Sakagami H, Mima K, Shiraga H, Azechi H, *submitted to Nucl. Fusion*

[29] Strozzi D J, Tabak M, Larson D J, Divol L, Kemp A J, Bellei C, Marinak M M, and Key M H 2012 Phys. Plasma **19** 072711

[30] Fujioka S, Zhang Z, Yamamoto N, Ohira S, Fujii Y, Ishihara K, Johzaki T, Sunahara A, Arikawa Y, Shigemori K, Hironaka Y, Sakawa Y, Nakata Y, Kawanaka J, Nagatomo H, Shiraga H, Miyanaga N, Norimatsu T, Nishimura H and Azechi H 2012 Plasma Phys. Control. Fusion **54** 124042

[31] Boehly T R, Brown D L, Craxton R S, Keck R L, Knauer J P, Kelly J H, Kessler T J, S. Kumpan A, Loucks S J, Letzring S A, Marshall F J, McCrory R L, Morse S F B, Seka W, Soures J M and Verdon C P 1997 Opt. Commun. **133** 495

[32] Stoeckl C, Cruz M, Glebov V Yu, Knauer J P, Lauck R, Marshall K, Mileham C, Sangster T C and Theobald W 2010 Rev. Sci. Instrum. **81** 10D302

[33] Theobald W, Ovchinnikov V, Ivancic S, Eichman B, Nilson P M, Delettrez J A, Yan R, Li G., Marshall F J, Meyerhofer D D, Myatt J F, Ren C, Sangster T C, Stoeckl C, Zuegel J D, Van Woerkom L, Freeman R R, Akli K U, Giraldez E, and Stephens R B, 2010 Phys. Plasmas **17** 103101

[34] Habara H, Adumi K, Yabuuchi T, Nakamura T, Chen Z L, Kashihara M, Kodama R, Kondo K, Kumar G R, Lei L A, Matsuoka T, Mima K and Tanaka K A 2006 Phys. Rev. Lett. **97** 095004

[35] Li J, Davies J R, Mori W B, Ren C, Solodov A A, Theobald W, Ma T and Tonge J, "Hot electron generation from laser-preplasma interactions in cone-guided fast ignition", *submitted to Physics of Plasmas*

[36] Radha P B, Collins T J B, Delettrez J A, Elbaz Y, Epstein R, Glebov V Yu, Goncharov V N, Keck R L, Knauer J P, Marozas J A, Marshall F J, McCrory R L, McKenty P W, Meyerhofer D D, Regan S P, Sangster T C, Seka W, Shvarts D, Skupsky S, Srebro Y and Stoeckl C 2005 Phys. Plasmas **12** 056307

[37] Shay H D, Amendt P, Clark D, Ho D, Key M, Koning J, Marinak M, Strozzi D and Tabak M 2012 Phys. Plasmas **19** 092706

[38] Hatchett S P, Clark D, Tabak M, Turner R E, Stoeckl C, Stephens R B, Shiraga H, Tanaka K 2006 Fusion Science and Technology **49** 327

[39] Shiraga H, Fujioka S, Jaanimagi P A, Stoeckl C, Stephens R B, Nagatomo H, Tanaka K A, Kodama R and Azechi H 2004 Review of Scientific Instruments, **75** 3921

[40] Stephens R B, Hatchett S P, Tabak M, Stoeckl C, Shiraga H, Fujioka S, Bonino M, Nikroo A, Petrasso R, Sangster T C, Smith J and Tanaka K A 2005 Phys. Plasmas **12** 056312

[41] Meyer-ter-Vehn J, and Schalk C 1982 Z. Naturforschung 1982 **37 A** 955

[42] Morreeuw J P and Saillard Y 1978 Nucl. Fusion **18** 1263

[43] Clark D S and Tabak M 2007 Nucl. Fusion **47** 1147

[44] Betti R and Zhou C 2005 Phys. Plasmas **12** 110702

[45] Tabak M, Clark D, Town R and Hatchett S 2007 BAPS.2007.DPP.GP8.40

[46] Tabak M, Shay H D, Strozzi D, Grote D, Larson D, Nuckolls J D and Zimmerman G B 2010 BAPS.2010.DPP.JP9.105

[47] Marinak M M, Kerbel G D, Gentile N A, Jones O, Munro D, Pollaine S, Dittrich T R and Haan S, 2001 Phys. Plasmas **8** 2275